Dendritic Growth of Undercooled Nickel-Tin: Part III

Y. WU, T. J. PICCONE, Y. SHIOHARA, and M. C. FLEMINGS

Studies were made of structure and solute distribution in undercooled droplets of nickel-25 wt pct tin alloy and the eutectic nickel-32.5 wt pct tin alloy. Structures of levitation melted droplets of the Ni-25 wt pct Sn alloy showed a gradual and continuous transition from dendritic to fine-grained spherical with increasing initial undercooling up to about 180 K. Results suggest that all samples solidified dendritically and that the final structures obtained were largely the result of ripening. Experimental data on minimum solute composition in the samples produced are bounded by two calculated curves, both of which assume equilibrium at all liquid-solid interfaces during recalescence and subsequent cooling. One assumes complete diffusion in the solid during recalescence; the other assumes limited diffusion, but partial remelting to avoid superheating of the solid. Several observations support the view that the eutectic alloy solidifies dendritically, much as the hypoeutectic alloy does. Surface dendrites were seen in regions of surface shrinkage cavities and a coarse "dendritic" structure can be discerned on polished sections, which seems to correspond to the large surface "dendrites" seen by high-speed photographs of the hypoeutectic alloy. The structure of highly undercooled eutectic samples is composed fully of an anomalous eutectic. Samples solidified with intermediate amounts of undercooling possess some lamellar eutectic which, it is believed, solidified after recalescence was complete.

I. INTRODUCTION

THIS is the third in a series of papers on dendritic growth and structure of undercooled nickel-tin alloys. In Part I,[1] cinematographic measurements of dendritic growth were reported and compared with the analyses of Lipton, Kurz, and Trivedi (LKT), and of Boettinger and Coriell (BC). The dendrite growth velocities measured agreed well with the LKT-BC theory, but the observed tip radii were several orders of magnitude larger than expected. It was concluded that the large dendrites observed comprised an array of much finer, solute diffusion controlled dendrites. In Part II,[2] high-speed thermal measurements were reported; these provided additional information on processes occurring behind the dendrite tips during and after recalescence. It was discovered that recalescence occurs in two stages. In the initial, rapid recalescence stage, an array of fine dendrites sweeps across the alloy sample. In the subsequent, slow stage of recalescence, the sample temperature rises slowly, following a relationship strongly suggestive of coarsening of the dendritic structure. The maximum recalescence temperatures reached by hypoeutectic Ni-25 pct Sn samples with different initial undercoolings were in good agreement with the equilibrium states predicted using a thermal balance combined with the equilibrium lever rule. A similar model appeared to apply for solidification of the Ni-32.5 pct Sn eutectic alloy. In this paper, we describe the structures and microsegregation measured in the samples produced, and relate these to the results of the previous two papers.

A number of studies have been reported on structure of undercooled iron and nickel base alloys, including nickel-tin. Walker[3] first reported the observation in pure nickel of a critical undercooling (about 170 K) at which grain size abruptly decreased. This critical undercooling was also observed in a number of iron and nickel base alloys by Kattamis and Flemings.[4,5,6] Their work and the later work by Kattamis and co-workers[7] showed that the dendritic structure gradually changes as this critical undercooling is approached, and at a critical undercooling is replaced by a spherical morphology, the size of which is on the order of the secondary dendrite arm spacing of the dendritic structure that has been replaced. Regardless of morphology, however, the important variable influencing dendrite element spacing is "local solidification time." Increasing undercooling decreases dendrite element spacing, but does so because it decreases "local solidification time."

Studies on solute redistribution in highly undercooled metal alloys have been reported, and a number of solidification models have been proposed.[4,8-11] Experiments on the distribution of nickel in highly undercooled Fe-25 wt pct Ni alloy revealed that solute concentration in most cases increased gradually from a minimum to a maximum with increasing distance from the center of a dendrite arm.[4,9-11] However, dendrite arms and spherical dendrite elements in this alloy were found to possess solute-rich cores when they were rapidly solidified after undercooling and nucleation. In some cases, the coring pattern outlined two or more small "dendrite arms" within the larger dendrite structure.[11] Fe-25 wt pct Ni alloy differs from the alloy in this study in that it has a narrow equilibrium solidification range, which allows a significant fraction of the initial solid which forms during recalescence to have the same composition as the initially undercooled bulk liquid. Therefore, steady state growth with local equilibrium at the interface is controlled by both thermal and solute diffusion. If growth is partitionless, which is probable for Fe-25 pct

Y. WU, formerly a Graduate Research Assistant in the Department of Materials Science and Engineering, Massachusetts Institute of Technology, Cambridge, MA 02139, is a Senior Engineer with ALCOA, Alcoa Center, PA 15069. T. J. PICCONE, Graduate Research Assistant, and M. C. FLEMINGS, Toyota Professor of Materials Processing and Department Head, are with the Department of Materials Science and Engineering, Massachusetts Institute of Technology, Cambridge, MA 02139. Y. SHIOHARA is a Research Associate in the Materials Processing Center, Massachusetts Institute of Technology, Cambridge, MA 02139, and also a Special Research Fellow at the Castings Research Laboratory of Waseda University, Tokyo, Japan.

Manuscript submitted April 27, 1987.

Ni with the high undercoolings attainable (about 300 K), growth will be controlled purely by thermal diffusion, resulting in higher growth rates than for concentrated Ni-Sn alloys (such as Ni-25 pct Sn).

Boettinger, Coriell, and Sekerka[12] have outlined the conditions for partitionless solidification (including solute trapping) using the thermodynamic considerations of Baker and Cahn[13] and the kinetic model of Aziz[14] for partition ratio as a function of interface velocity. For a typical metallic system, they estimated that the lower limit for the critical velocity necessary to achieve partitionless solidification is about 2 m/s for plane front growth. For dendritic growth, the critical velocity is expected to be higher than this value, due to the three-dimensional nature of the solute diffusion.

Iron and nickel base alloys are often used for undercooling experiments because they can be made to undercool by large amounts relatively easily. However, lower melting point metals, particularly lead and tin alloys, can also be readily undercooled and are amenable to undercooling studies using the emulsion technique. Studies on structures of such alloys have been reported.[15,16,17]

Many studies have also been reported on solidification of rapidly solidified atomized droplets. When structures are significantly different from the usual dendritic type, it has often been assumed that significant undercooling took place before nucleation.[8,18–20]

II. EXPERIMENTS

Undercooling experiments on nickel-tin alloys were performed using an apparatus consisting of a high-frequency levitation melter, a two-color pyrometer, and a data storage and manipulation system. The experimental apparatus and procedures have been described in detail in a separate paper.[2] The metal samples were nickel-tin alloys: Ni-25 wt pct Sn hypoeutectic alloy and Ni-32.5 wt pct Sn eutectic alloy. Samples of approximately 9 mm diameter (3.2 g) were melted and cooled within a borosilicate glass medium. After completion of a run, the glass surrounding the metal sample was removed, and the sample was then cleaned in an ultrasonic cleaner in acetone. Surface and cross-sectional microstructures were examined using scanning electron microscopy (SEM). A thin layer of gold was applied by evaporation for surface examination. The cross-sectional structures of undercooled Ni-25 wt pct Sn alloy samples were sometimes revealed using the SEM in backscattered mode without prior etching. In all other cases, a dilute solution of Marble's reagent (4 g $CuSO_4$, 20 cc HCl, and 20 cc H_2O, mixed with distilled water in a ratio of 1 part etchant to 6 parts water) was the etchant used to reveal the microstructures of the undercooled samples. The etching time was a few seconds.

Several runs were also made using 3 mm diameter (0.2 g) samples in a DTA (Differential Thermal Analysis) apparatus in order to obtain structures of samples cooled at slower rates than those described above. Samples produced in this way were used only for "dendrite element" spacing measurements. These samples were solidified in the DTA with initial undercoolings up to 80 K and at controlled cooling rates from 2 to 30 K/min.

Solute distribution was measured using a Cameca Camebax electron microprobe. An acceleration voltage of 20 kV and a beam current of 20 nA were employed during point counting, integrating for 15 seconds for each element. The "take-off" angle for the microprobe was 40 deg.

III. RESULTS

A. *Dendrite Structure and Spacing, Ni-25 Wt Pct Sn Alloy*

The microstructure of undercooled Ni-25 wt pct Sn hypoeutectic alloy was found to exhibit a morphology transition from a typical dendritic structure at low undercoolings to a spherical, nondendritic structure at high undercoolings, as can be seen in Figures 1 and 2. In the samples shown in Figures 1(a) and 1(b), which were undercooled 62 and 112 K, respectively, the microstructures consist of typical branched dendrites of the primary nickel-rich phase and interdendritic eutectic. In the samples shown in Figures 1(c) and 1(d), which were undercooled 183 and 324 K, respectively, the microstructures are composed of randomly oriented fine spherical grains or "dendrite elements" of nickel-rich α-phase surrounded by the eutectic in the central region and by divorced eutectic (Ni_3Sn β-phase) in regions near the surface. The morphological transition from a branched dendritic structure to the fine spherical "dendrite element" structure in this alloy occurred gradually and continuously over the entire range of undercoolings up to about 180 K, where it was largely complete. This gradual morphological transition is strongly suggestive of a ripening mechanism being largely responsible for the final structures observed.

One interesting observation using the SEM in the backscattered mode was the contrast difference observed in dendrite arms and in spherical dendrite elements. In samples with low undercoolings, the contrast difference was observed as solute-poor cores in dendrite arms; no contrast difference was observed between neighboring dendrite arms of the same grain, as shown in Figure 1(a). However, large differences in contrast were observed between spherical "dendrite elements" in samples with high undercoolings, as shown in Figure 1(c). When these dendrite elements are connected to each other, the boundary of the contrast difference is always at the neck. Quantitative measurements show the existence of only small solute concentration differences across dendrite elements and similar solute distribution patterns in different dendrite elements in the same sample. Thus, the difference in contrast between dendrite elements must result from a difference in the orientations of these elements,[21,22] *i.e.*, of different grains. In Figure 1(d), the contrast due to differences in orientation is not so evident because the grains are smaller. At higher magnification (see Figure 6(a)), the contrast difference in this sample is more easily observed.

Regardless of morphology, the microstructure becomes finer with increasing initial undercooling, as can be seen in Figures 1 and 2. Measurements were made of the dendrite element spacings (secondary dendrite arm spacing for dendritic samples or spacing of spherical elements for nondendritic samples) near the surface of the sample. The dependence of these arm spacings on time for solidification of the primary phase is shown in Figure 3. This time was measured from the first nucleation event to the second nucleation event on cooling of each undercooled Ni-25 wt pct Sn hypoeutectic alloy sample; it decreases linearly with

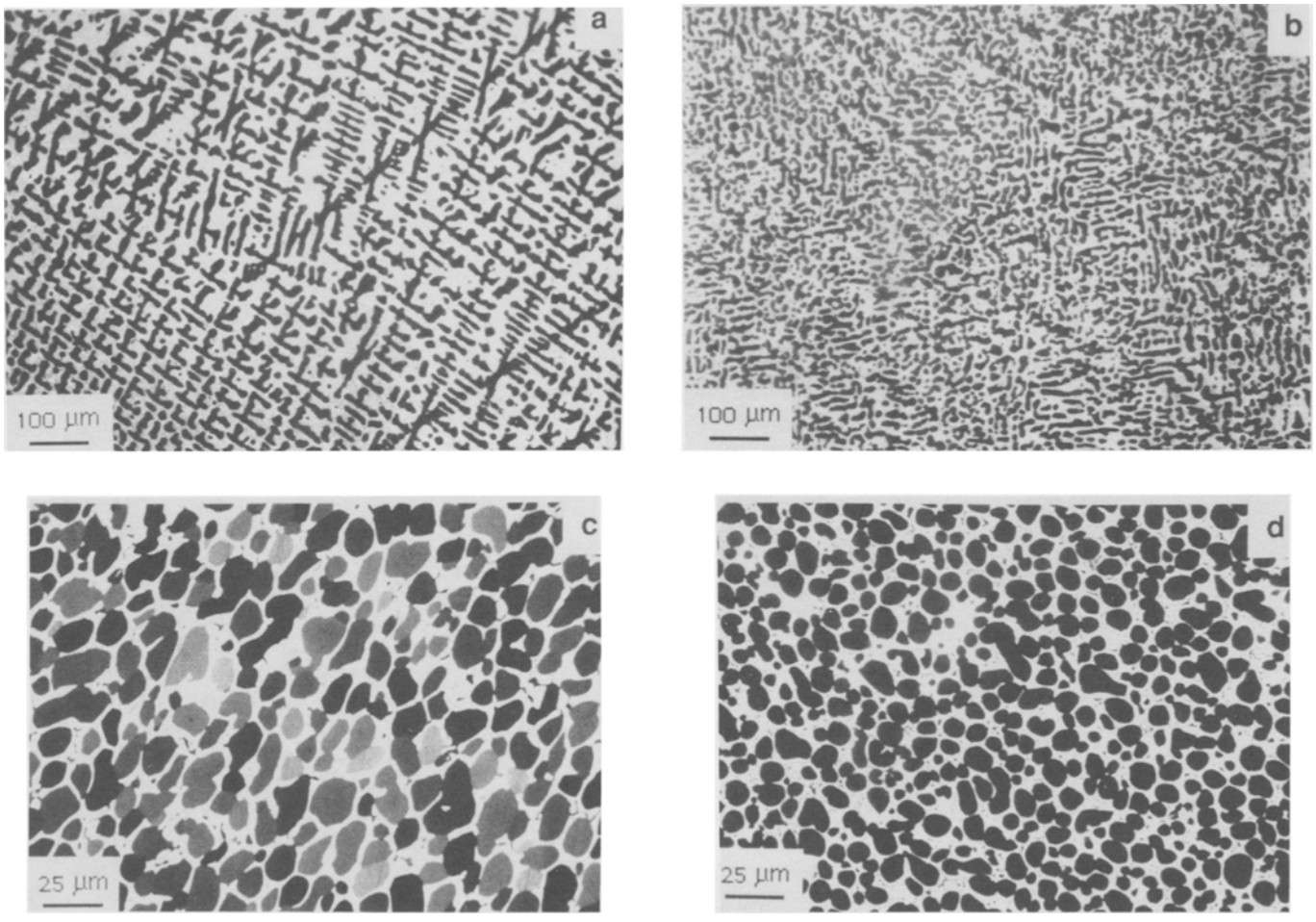

Fig. 1 — Cross-sectional microstructures of four Ni-25 wt pct Sn hypoeutectic alloy samples with different initial undercoolings, showing the gradual morphology transition from dendritic to spherical with increasing undercooling. Undercoolings: (*a*) 62 K, (*b*) 112 K, (*c*) 183 K, and (*d*) 324 K.

increasing initial undercooling for levitation melted samples, as described in a separate paper.[2] As will be shown later, this time corresponds to total solidification time for the primary phase, t_p, at the sample surface. Also plotted in Figure 3 are results of the experiments performed using the DTA on small droplets (3 mm in diameter) of the same alloy. In the DTA results, solidification time varied with both undercooling and the controlled cooling rate. Experimental conditions and data used to plot Figure 3 are summarized in Table I. Regardless of solidification conditions, *i.e.*, amount of undercooling, cooling rate, or sample size, the data nearly all fall on the same curve, a straight line with a slope of 0.36, indicating that ripening is the controlling factor in determining the dendrite element spacing. The dendrite element spacing for the levitation melted sample with 324 K initial undercooling has not been plotted in Figure 2, since it was not possible to determine the primary phase solidification time. However, Figure 4 shows that the dendrite element spacing at the surface of that sample is about 1 μm, which seems to agree well with the relationship found for the other samples.

The structures shown in Figure 1 and the data plotted in Figure 3 are for regions at or near the surfaces of the approximately spherical specimens. Dendrite element spacings were found to increase significantly with distance radially inward from the surface. Figure 4, for example, shows measurements of the dendrite element spacing on a cross section of a Ni-25 wt pct Sn hypoeutectic alloy sample undercooled 324 K. Measurements were made along a diameter of the sample cross-section. The five photographs shown were taken from locations A to E along the diameter, as labeled.

It is at first surprising to see this large difference in spacing from surface to center, since the cooling in these samples after recalescence is approximately Newtonian (as discussed in a separate paper[2]), and so the cooling rate is nearly the same at the center as at the surface. The explanation of the obtained results is that, although the cooling rate is essentially the same at center and surface, the large amount of eutectic present in the sample results in a "local solidification time" that is much longer at the center than at the surface of the sample.

Neglecting the small recalescence time, local solidification time, t_f, is the sum of the time for solidification of the primary phase after recalescence, t_p (if any), and the time for solidification of the eutectic, t_E:

$$t_f = t_p + t_E \qquad [1]$$

For Newtonian cooling, t_p is independent of location in the sample. The time t_E is the time after t_p required for the

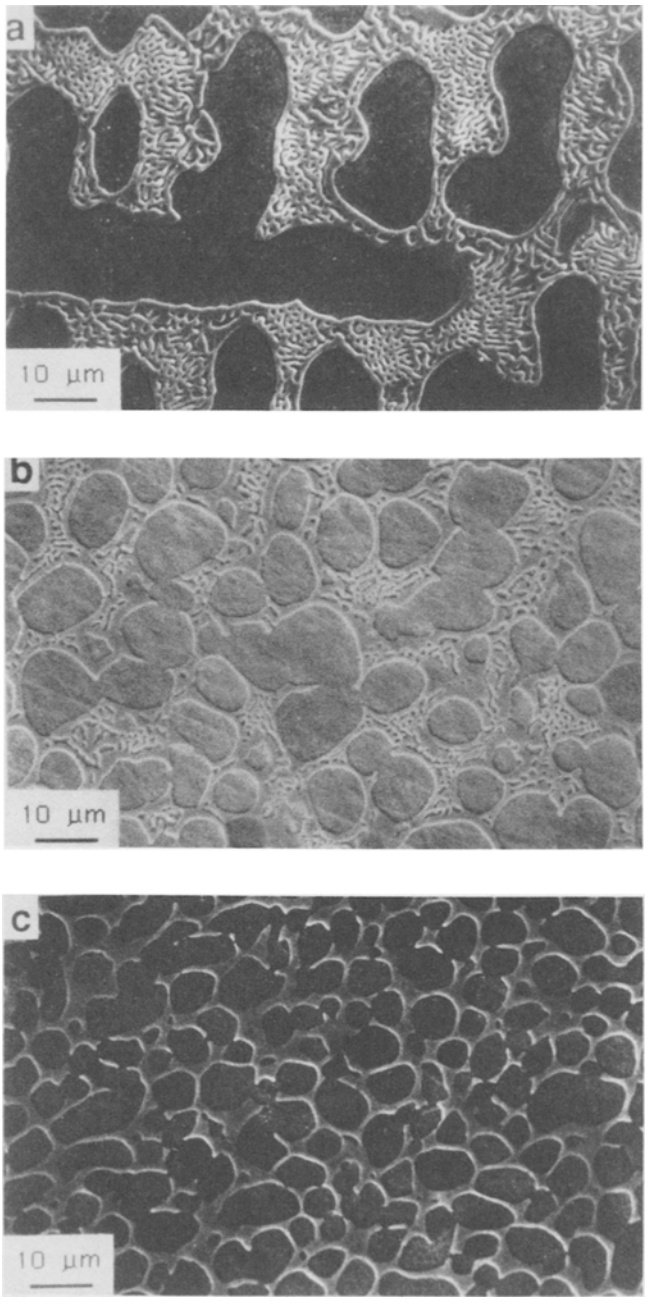

Fig. 2—Cross-sectional microstructures of three Ni-25 wt pct Sn hypoeutectic alloy samples with different initial undercoolings, showing the interdendritic structures. Undercoolings: (*a*) 112 K, (*b*) 183 K, and (*c*) 324 K.

eutectic solidification front to reach the given radial location, r. For a constant rate of heat extraction at the sample surface, and for solidification progressing radially inward, t_E is given by the relation:

$$\frac{t_E}{t_{Ef}} = 1 - \left(\frac{r}{r_0}\right)^3 \qquad [2]$$

where r_0 is sample radius and t_{Ef} is the time required for the eutectic front to reach the center of the sphere. The dendrite arm spacing, d, of the primary phase is given by the usual relation, shown in Figure 3:

$$d = a(t_f)^n \qquad [3]$$

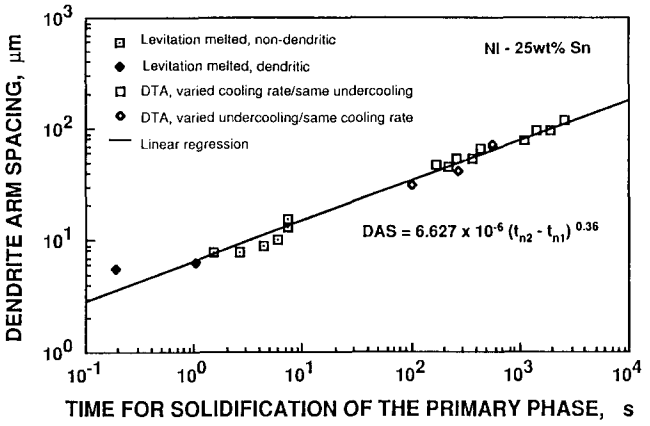

Fig. 3—Log-log plot of secondary dendrite arm spacing *vs* time for primary phase solidification.

where a and n are constants. Combining Eqs. [1], [2], and [3] yields the following relation for d *vs* r:

$$d = a\{t_p + t_{Ef}[1 - (r/r_0)^3]\}^n \qquad [4]$$

Figure 4 includes a plot of Eq. [4] above, for d *vs* r/r_0 for the Ni-25 wt pct Sn sample. In this calculation, a and n were determined from the experimental data of Figure 3 ($a = 6.63 \times 10^{-6}$ m, and $n = 0.36$), and t_{Ef} was obtained from optically measured cooling curves of the type presented in a previous paper.[2] The solidification time after recalescence for the primary phase, t_p, is zero for this high undercooling. The additional time t_{Ef} is the measured eu-

Table I. Dendrite Element Spacing in Ni-25 Wt Pct Sn Samples

Sample Type	Initial Undercooling (K)	Time for Solid'n of Primary Phase (s)	Dendrite Element Spacing (μm)
L-M Samples			
9 mm dia.	62	6.88	14.9
9 mm dia.	76	6.63	12.9
9 mm dia.	85	7.39	15.2
9 mm dia.	112	5.85	11.8
9 mm dia.	138	4.32	9.0
9 mm dia.	183	2.67	7.7
9 mm dia.	211	1.52	7.8
9 mm dia.	235	1.02	6.2
9 mm dia.	262	0.19	5.5
DTA Samples			
3 mm dia.	5	426	66.25
3 mm dia.	8	264	53.44
3 mm dia.	8	170	46.25
3 mm dia.	8	1080	79.06
3 mm dia.	6	2580	118.75
3 mm dia.	10	368	54.38
3 mm dia.	17	223	44.38
3 mm dia.	8	1395	96.88
3 mm dia.	7	1900	96.88
3 mm dia.	80	102	31
3 mm dia.	13	552	69
3 mm dia.	6	564	73
3 mm dia.	33	276	41

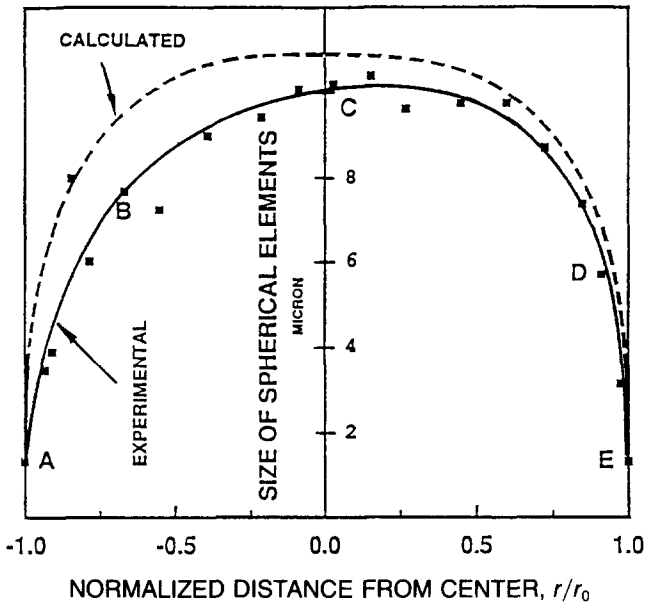

(*a*)

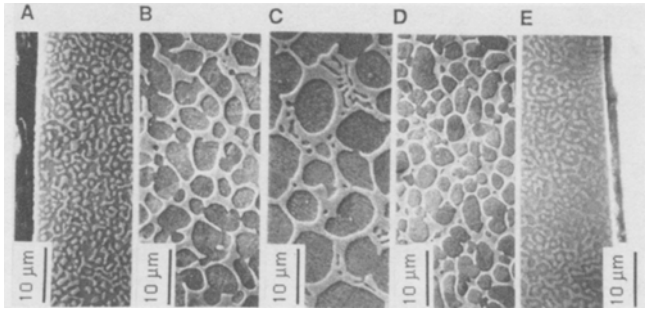

(*b*)

Fig. 4—Dependence of diameter of spherical elements on position in a Ni-25 wt pct Sn hypoeutectic alloy sample undercooled 324 K. The five photographs correspond to the five data points labeled in the plot.

tectic "hold," and was 4.01 seconds for this sample. These numbers can be obtained from Figure 5 in Reference 2. The resulting calculated curve in Figure 4 shows quite good agreement with experiment.

B. *Solute Distribution, Ni-25 Wt Pct Sn Alloy*

Quantitative measurements of solute concentration in the dendrites were made using electron microprobe analysis (EMPA). Analyses were taken at individual points, integrating the signals for 15 seconds for each element. The distance between points was one micron. A typical profile across a dendrite arm is shown in Figure 5; it was obtained from a region near the center of a sample undercooled 62 K. The solute concentration increases radially outward in the dendrite arm. Figure 6 is a composition profile obtained from a typically highly undercooled sample. This specimen, undercooled 324 K, shows negligible segregation of solute in the spherical "dendrite element." The interdendritic compositional peaks are in the second phase. The solute concentration in the spherical elements was about 19 wt pct Sn, and the composition of the second phase was 40 wt pct Sn. These are the compositions of the two phases at equilibrium at the eutectic temperature.

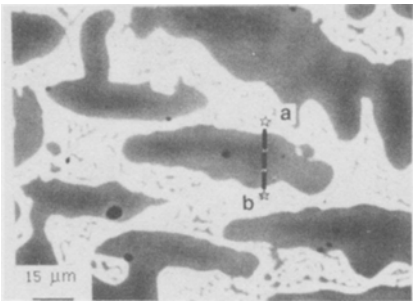

(*a*)

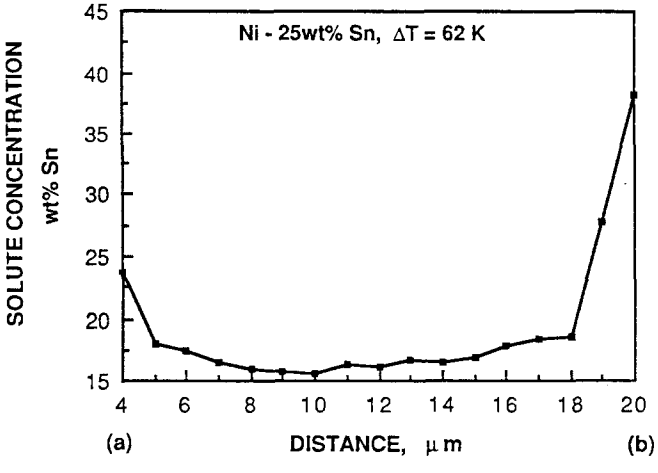

(*b*)

Fig. 5—Composition profile across a dendrite arm in Ni-25 wt pct Sn undercooled 62 K.

Minimum solute concentration in a given sample must be determined by a trial and error method, because of the difficulty of finding the exact minimum. For each minimum determined in this work, solutal distributions were measured across approximately 20 dendrite arms (or spherical dendrite elements), the lowest solute concentration was determined in each arm, and the lowest of these was taken as the measured minimum for the sample. These minimum measured compositions for a number of such samples are plotted *vs* sample undercooling in Figure 7, and compared with two calculated curves discussed below.

The first of these curves, Curve 1, was calculated by applying the solidification model described in a separate paper[2] in the simplest possible way, that is, by assuming equilibrium of a homogeneous, continuous solid phase with its surrounding liquid at the "maximum local recalescence temperature." The "maximum local recalescence temperature" is the maximum temperature reached behind the growing dendrite tip during recalescence and subsequent cooling. It is taken to be equal to the maximum adiabatic recalescence temperature, calculated as discussed in the Appendix. Curve 1 places a lower bound on our experimental results in Figure 7.

We may now consider another possibility, still assuming equilibrium of liquid and solid at the maximum recalescence temperature. The "solidification path" proposed in a previous paper[2] is assumed, but it is also assumed that solid state diffusion is sufficiently slow that the solid cannot adjust its composition over the entire dendrite arm diam-

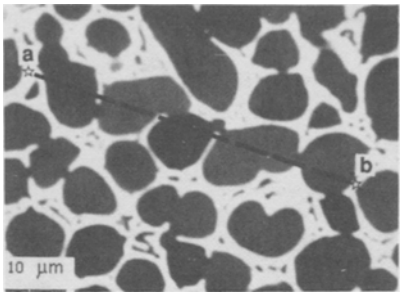

(*a*)

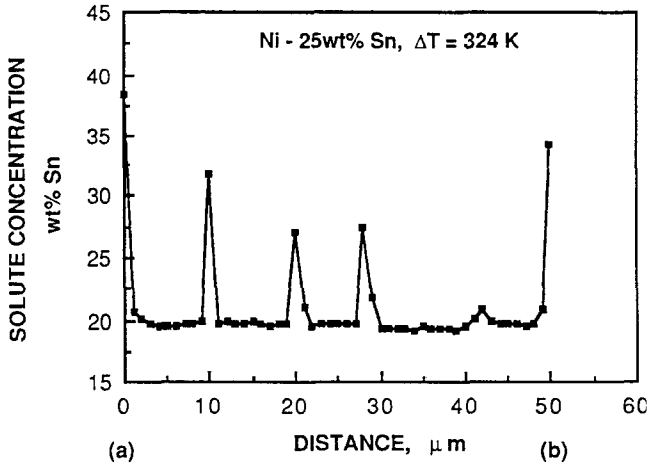

(*b*)

Fig. 6—Composition profile across five spherical dendrite elements in Ni-25 wt pct Sn undercooled 324 K.

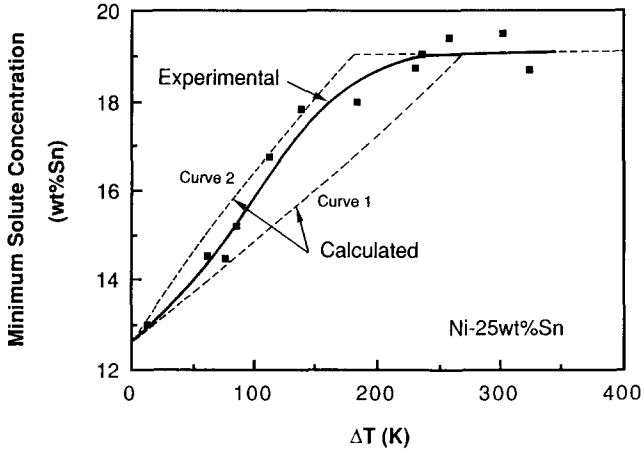

Fig. 7—Minimum solute concentration *vs* undercooling for Ni-25 wt pct Sn alloy.

eter to the changing equilibrium solid composition. Instead, the solid within the dendrite is assumed to remelt partially in small closely spaced pockets that are not directly connected with the interdendritic liquid. The result is that the sample recalesces to the same maximum temperature as it would if diffusion in the solid were infinitely fast, and the resulting liquid and solid are again at their equilibrium compositions and temperature. However, the liquid remaining at this temperature is of two types, one the usual interdendritic liquid, and the other the small isolated pockets of liquid within the dendrites. If sufficiently fine, these small pockets would disappear by solid state diffusion during the relatively slow solidification (after recalescence) of these experiments. The result would be solute enriched dendrites, or at least solute enriched dendrite cores. This possibility has been considered qualitatively previously in a separate paper,[2] and calculations describing it for Ni-25 wt pct Sn are given in the Appendix. The results of the calculations are given in Curve 2 of Figure 7; they provide an upper limit for our experimental results.

C. *Ni-32.5 Wt Pct Sn Eutectic Alloy*

The microstructure of the eutectic alloy, like Ni-25 wt pct Sn hypoeutectic alloy, is significantly affected by undercooling. In general, the microstructure of an undercooled eutectic sample consists of two distinguishable regions: normal lamellar eutectic and anomalous eutectic.

Figure 8 shows microstructures for three Ni-32.5 wt pct Sn eutectic alloy samples with different initial undercoolings. At low undercooling, Figure 8(a), the structure is fine lamellar eutectic. The lamellae are coarser and shorter at intermediate undercooling, Figure 8(b). At high undercooling, the structure is very fine anomalous eutectic, Figure 8(c).

The cause of the microstructural coarsening in Figure 8(b), in comparison with Figure 8(a), consists in a difference in the solidification mechanism. The lamellar eutectic solidifies with the two solid phases growing simultaneously with a macroscopically planar front. The spacing of the lamellae is determined by lateral diffusion at the interface. Since there is no liquid in contact with the growing solid phases except at the interface, significant coarsening does not occur, and the final lamellar spacing is small. The anomalous eutectic, however, forms by the growth, remelting, and decomposition of primary supersaturated dendrites. As in the solidification of the hypoeutectic alloy mentioned earlier, coarsening occurs because the dendritic solid and interdendritic liquid phases coexist for some time before solidification is complete. This explains the trend from fine lamellae to short, coarse lamellae to fine anomalous eutectic with increasing initial undercooling.

One interesting observation of surface morphology of these eutectic alloy samples was the well-oriented, two-phase dendritic structure which could often be obtained. This structure could even be observed at high undercoolings (>200 K), although no trace of such a structure was observed within the sample itself. Figure 9 shows such a structure for a eutectic alloy sample undercooled 220 K. The two phases (α and β) are both present in these dendrites, which have secondary branches at regular spacing on their main branches in a well-oriented manner with an angle of about 70 deg.

At low undercoolings, the structure within the samples is largely lamellar eutectic, as in Figure 8(a). At intermediate undercoolings, the structure is composed of two regions. At low magnification, one of these regions is seen to have the appearance of a dendrite-like structure, as in Figure 10(a). At high magnification, Figure 10(b), this region is seen to comprise a two-phase structure conforming to the classical term of "anomalous eutectic." These two-

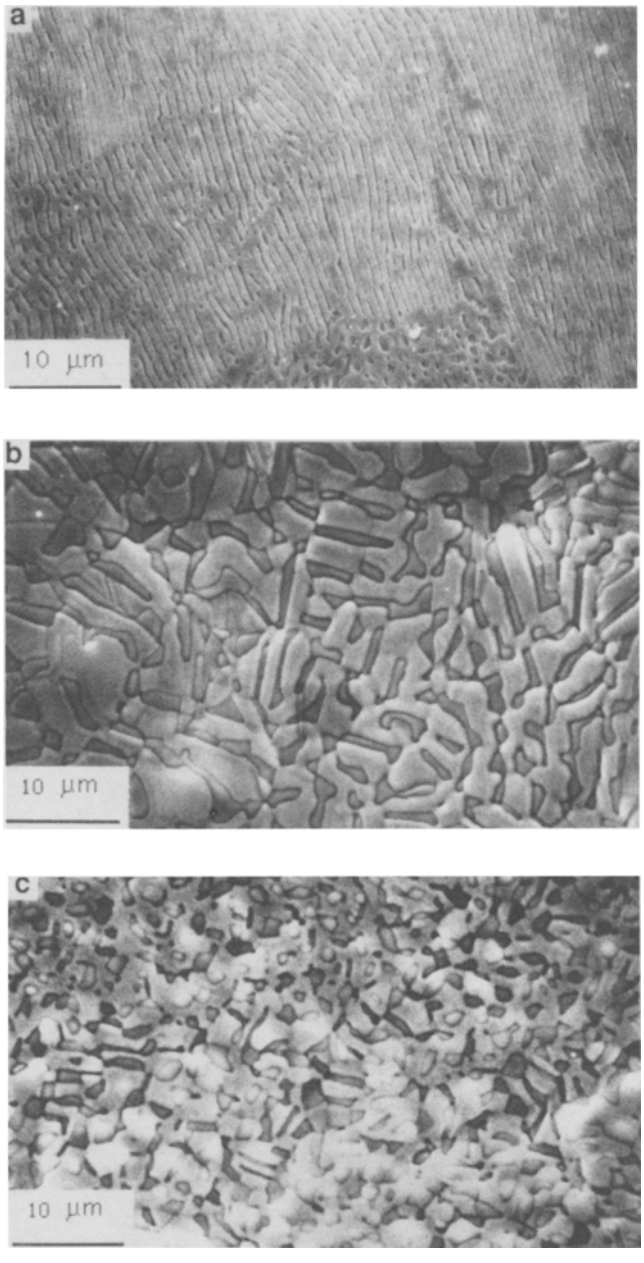

Fig. 8—Morphologies of three Ni-32.5 wt pct Sn eutectic alloy samples with different initial undercoolings. Undercoolings: (*a*) 31 K, (*b*) 140 K, and (*c*) 225 K.

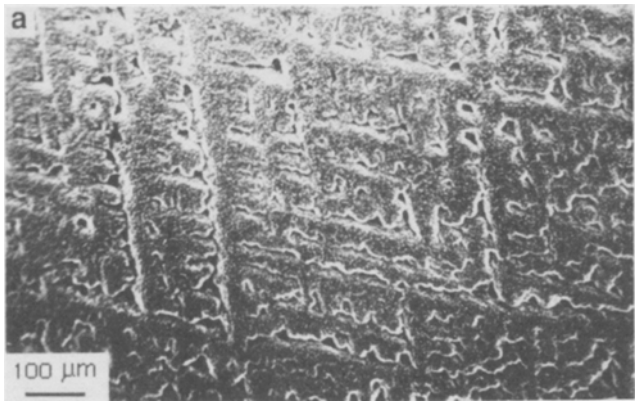

Fig. 9—Well-oriented two-phase dendritic structure observed on the surface of a Ni-32.5 wt pct Sn eutectic alloy sample undercooled 220 K.

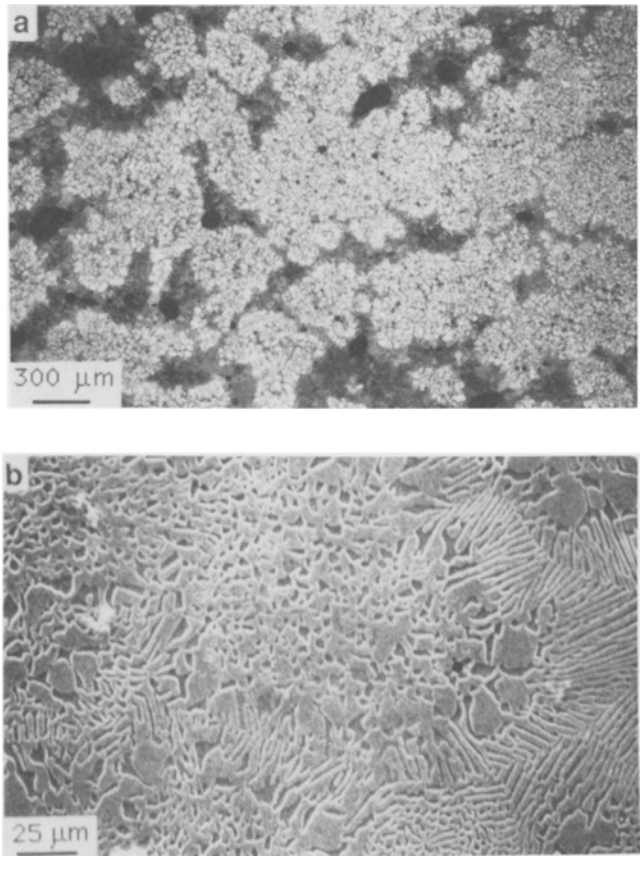

Fig. 10—Cross-sectional microstructures of two Ni-32.5 wt pct Sn eutectic alloy samples with different undercoolings, showing the dendrite-like appearance of the anomalous eutectic regions. Undercoolings: (*a*) 31 K and (*b*) 113 K.

phase dendrite-like structures in Figure 10(a) have been termed "ghost dendrites".[23] The darker phase was determined by EMPA to be nickel-rich and the lighter phase to be Ni_3Sn. Outside this region, the remainder of the structure is normal lamellar eutectic. The arm spacing of these ghost dendrites could be measured, at least approximately; this spacing decreased with increasing initial undercooling, as shown in Figure 11. Also plotted, for comparison, are "dendrite" arm spacings measured cinematographically for undercooled Ni-25 wt pct Sn alloy, as described earlier in a separate paper.[1] The two sets of data form a smooth, continuous curve.

The average size of the nickel-rich particulates increases significantly from surface to center of a sample. Figure 12 shows two microstructures of a Ni-32.5 wt pct Sn eutectic alloy sample undercooled 113 K, one from a region very close to the sample surface and the other from near its center. The large size difference of these particulates is apparent, and this difference is presumably due to ripening of the two-phase structure.

The volume fraction of lamellar eutectic was measured by point counting,[24] with the total number of points being in the range of 2000 to 3000 per sample. In samples with

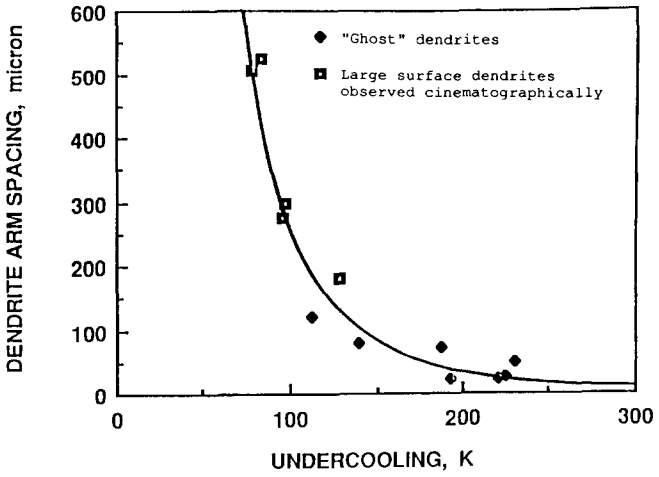

Fig. 11 — Measured ghost dendrite arm spacing *vs* undercooling for Ni-32.5 wt pct Sn eutectic alloy samples. Results are compared with dendrite arm spacings for Ni-25 wt pct Sn alloy estimated from photography.

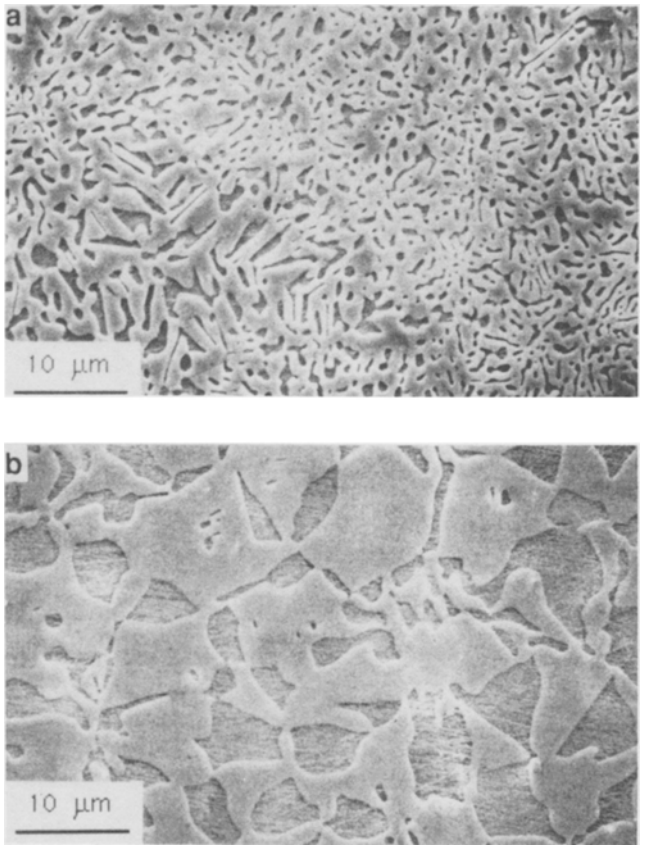

Fig. 12 — Microstructures of a Ni-32.5 wt pct Sn eutectic alloy sample undercooled 113 K: (*a*) in a region near the sample surface, and (*b*) in a region near its center, showing the large size difference of nickel-rich α-phase particulates.

high undercoolings, lamellar eutectic could be observed only at high magnification. The volume fraction of lamellar eutectic was found to decrease with increasing initial undercooling as shown in Figure 13.

Figure 14 shows results of composition analyses on the dark and light phases in an anomalous eutectic region. Again, the phases are of the equilibrium compositions at the eutectic temperature, 19 wt pct and 40 wt pct Sn.

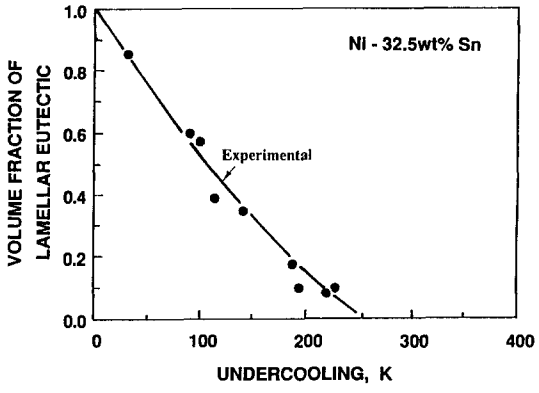

Fig. 13 — Volume fraction of lamellar eutectic structure *vs* undercooling for Ni-32.5 wt pct Sn alloy samples.

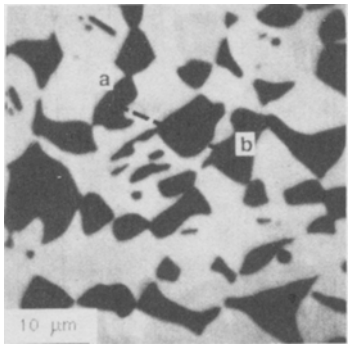

(*a*)

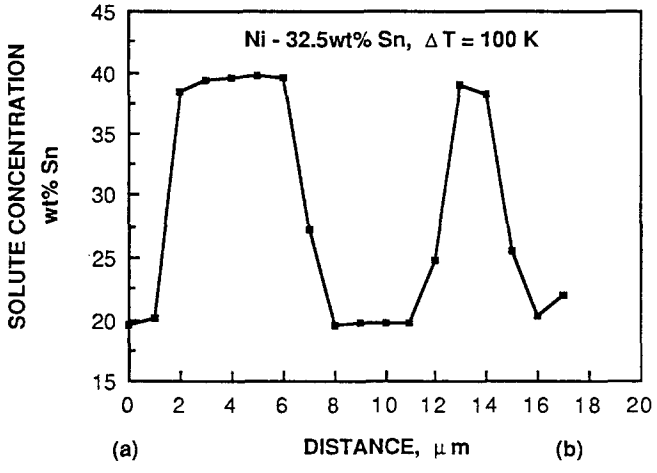

(*b*)

Fig. 14 — Composition profile in an anomalous eutectic region in Ni-32.5 wt pct Sn undercooled 100 K.

Analysis of average composition using a measurement area of 12 μm × 12 μm along a line across anomalous regions was made on some undercooled eutectic samples. Figure 15 is a typical result obtained from a sample undercooled 100 K. Taking into account the error introduced by randomly selecting areas which may cover either more nickel-rich phase or more Ni_3Sn phase, it can be concluded that there are no overall composition gradients in anomalous eutectic regions. A least-squares line through these data gives an average solute concentration of 32.5 wt

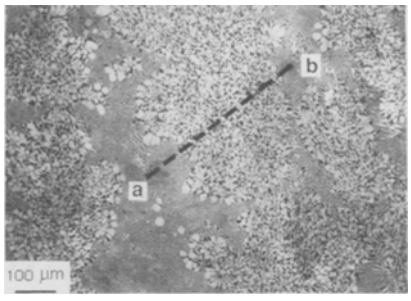

(*a*)

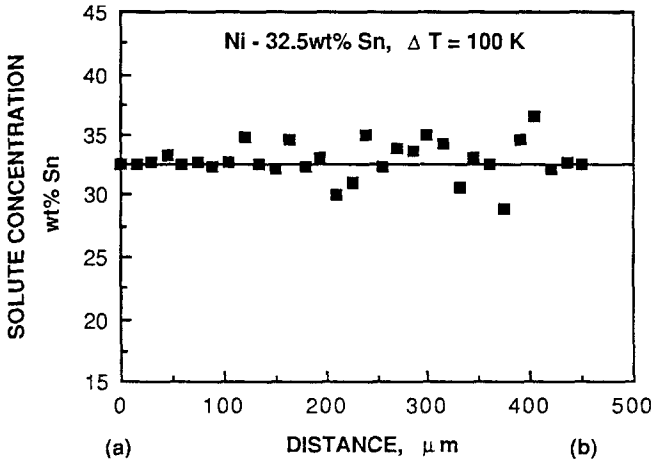

(*b*)

Fig. 15—Composition profile across an anomalous eutectic region in Ni-32.5 wt pct Sn undercooled 100 K.

pct Sn, which is exactly the eutectic composition. Thus, it is concluded that there is no composition difference between anomalous and normal lamellar eutectic regions, and that the ghost dendrites must have grown in such a way that their final average composition is just that of the eutectic.

We conclude that these large two-phase "dendrites" are remnants of the original growth structure, which we assume to have been dendrites of α growing into the undercooled melt, with β phase growing behind the α tips. Supporting this conclusion is the fact that tip velocities calculated for the eutectic alloy on the basis of the recalescence behavior discussed in a previous paper[2] is equal to the velocity calculated for growth of α dendrites according to the Lipton, Kurz, Trivedi analysis.[1,2] These ghost dendrites, especially at low undercoolings, occupy only a portion of the microstructural cross-section. We believe that at the end of recalescence they extend across the entire cross-section, but contract by sintering during subsequent cooling. Such rapid compaction of dendrites after recalescence has been demonstrated by Chu *et al.*[18]

The structures observed in this work are clearly determined primarily by time-dependent, surface energy-driven processes. Studies that combine controlled undercooling with more rapid rates of heat extraction are desirable to delineate the original solidification structure, and the evolution of that structure with time during solidification.

IV. SUMMARY AND CONCLUSIONS

1. There is a morphology transition from branched dendrites to spherical elements with increasing initial undercooling, which is complete below about 180 K undercooling in Ni-25 wt pct Sn alloy. The spherical morphology is thought to be the result of ripening after recalescence.
2. Ripening is the controlling factor in determining dendrite element spacing in the final microstructure.
3. Cooling of samples after recalescence is close to Newtonian; nonetheless, dendrite element spacing in Ni-25 wt pct Sn samples increased from the surface to the sample center. This is because substantial eutectic was present, so that final solidification was by a eutectic front advancing radially inward. Hence, the local solidification time was longer at the sample center than at the surface.
4. Minimum solute concentration within the dendrite elements increased with increasing undercooling from approximately kC_0 at low undercoolings to the maximum solubility limit at an undercooling of about 200 K.
5. Experimental data on minimum solute concentration were bracketed by two curves calculated on the assumptions, respectively, of (1) complete solid diffusion during recalescence, and (2) limited solid diffusion but partial internal remelting of the dendrite during recalescence, with entrapment of the liquid pools in the dendrite. Both calculations assume dendritic growth in accordance with the LKT model, that recalescence occurs with equilibrium at all liquid-solid interfaces, and that there is limited diffusion in the solid after recalescence.
6. The results show good agreement with the Lipton-Kurz-Trivedi model for steady state dendrite growth, which includes the assumption of local equilibrium at the solid-liquid interface. Although the presence of nonequilibrium effects at the interface during recalescence in the samples studied in this work cannot be ruled out, there is nothing in the results which confirms that such effects are present.
7. The eutectic alloy (Ni-32.5 wt pct Sn) samples often show a dendritic structure over the surface in areas where surface shrinkage is present. Similar dendrite-like structures are seen at low magnification on polished cross-sections. These dendritic areas are made up of two finely distributed phases and are of the overall bulk composition. This structure appears to be the remnant of an original growth structure in which only limited ripening occurred, due to the rapid removal of interdendritic liquid by shrinkage.
8. The arm spacing of the outlines of these ghost dendrites is several hundred microns. Plotted against undercooling, the spacings form a continuous, monotonically decreasing curve with similar data obtained from high-speed cinematographic measurements of dendrite growth in Ni-25 wt pct Sn. Thus, these also appear to be manifestations of the original growth structure—presumably α dendrites, with infilling by β growing behind the α dendrite tips.
9. On cross-sections, the regions between these ghost dendrites are lamellar. This portion of the structure presumably solidified after all undercooling was dissipated. The amount of lamellar eutectic decreases with increasing undercooling.

APPENDIX

Calculations of minimum solute concentration

As described in a separate paper,[2] the maximum adiabatic recalescence temperature, T_R, liquid composition, C_L^R, solid composition, C_s^R, and fraction of solid, f_s^R, at the maximum recalescence temperature can be calculated in terms of nucleation temperature, T_n, by solving the following equations:

$$f_s^R = \frac{C_p}{\Delta H}(T_R - T_n) \qquad [A1]$$

$$f_s^R = \frac{C_L^R - C_0}{C_L^R - C_s^R} \qquad [A2]$$

where C_p and ΔH are specific heat and latent heat of fusion of the alloy, respectively, and C_0 is the initial composition of the alloy. Assumptions made in the above equations include (1) adiabatic recalescence, (2) specific heats are the same for both solid and liquid and latent heat of fusion is independent of temperature, and (3) equilibrium of a homogeneous, continuous solid at the maximum recalescence temperature. Results of calculations using only Eqs. [A1] and [A2] yield the minimum possible solute concentration in the solid for a given undercooling; this is plotted as Curve (1) in Figure 7.

If diffusion in the solid over distances on the order of the dendrite element radius is limited, then superheating of the solid will result, unless remelting occurs. Suppose now that such remelting does occur, and that it occurs on a sufficiently fine scale that diffusion in the solid between the resulting liquid pools is essentially complete. The amount of remelted liquid varies from a maximum at the dendrite element center to a minimum of zero at the element surface at any time during recalescence above the solidus. Let the fraction of the sample comprising the partially remelted dendrite be f_d, and the remelted pools be a fraction f_L' of the total, or f_L'/f_d of the dendrite element. Then,

$$f_L = \overline{f_L'} + f_L'' \qquad [A3]$$

$$f_d = \overline{f_L'} + f_s \qquad [A4]$$

$$f_d + f_L'' = 1 \qquad [A5]$$

where f_L is the total fraction of liquid, f_L'' is the fraction of interdendritic liquid, and f_s is the fraction of solid.

Neglecting the effect of curvature, the solid composition at the liquid-solid interface is an isoconcentrate, C_s^i, which is the equilibrium solidus composition at the temperature of the interface. This isoconcentrate encloses a fraction of solid, f_d. As the temperature increases (the dendrite element grows), this surface (no longer at the interface, but within the solid dendrite) remains, on the average, an isoconcentrate, but partial remelting occurs so that a fraction f_L' of this defined "surface" is liquid. The small liquid pools are of composition C_L, and the solid of composition C_s, both of these being the equilibrium compositions at the temperature T of the growing dendrite element. A solute balance at this "surface" enclosing a fraction f then gives:

$$f_L' = \frac{C_s^i - C_s}{C_L - C_s} \qquad [A6]$$

Then the total fraction of remelted liquid, f_L' is:

$$\overline{f_L'} = \int_0^{f_d} f_L' \, df \qquad [A7]$$

From a thermal balance,

$$df_s = \frac{C_p}{\Delta H} dT \qquad [A8]$$

where C_p is the specific heat of the solid and liquid alloy, and ΔH is the heat of fusion.

Equations [A1] and [A2] give the fraction solid, f_s^R, at the maximum recalescence temperature, and the maximum recalescence temperature. These are the same as in the simpler case of complete solid diffusion, which was discussed earlier. Equations [A3] to [A8] can be solved numerically to give f_L' and f_L'' (or f_d) at any temperature during recalescence, including the maximum recalescence temperature. For low to intermediate undercoolings, the solidification "path" of the liquid and solid compositions is given simply by the liquidus and solidus of the phase diagram. Equations describing the liquidus and solidus for the nickel-tin system have been given in an earlier paper.[2]

For undercoolings greater than 220 K (for Ni-25 pct Sn alloy), undercooling due to thermal diffusion begins to become significant. The thermal undercooling, ΔT_α, results in a fraction solid, f_s°, forming at a tip of composition C_l, where:

$$f_s^\circ = \frac{C_p \, \Delta T_\alpha}{\Delta H} \qquad [A9]$$

Undercooling due to radius of curvature alters the "solidification path" by lowering the equilibrium solidus and liquidus of the curved surface. In these calculations, we have taken the path to be that shown schematically in Figure 13 in Reference 2. The solidus and liquidus are assumed to be lowered an amount ΔT_r at T_n and $1/2\ \Delta T_r$ at the maximum temperature of rapid recalescence, T_R'. The latent heat of fusion employed in the calculations is reduced from the actual value by the small fraction $(T_R - T_R')/(T_R - T_n)$ to account for the residual heat evolved during slow recalescence from T_R' to T_R as a result of coarsening.

Now, at the maximum recalescence temperature, T_R, the dendrite of fraction f_d has a distribution of remelted liquid of fraction f_L', varying from a maximum at its center to zero at its surface. Its average composition, $\overline{C_{sd}}$, is given by:

$$\overline{C_{sd}} = \frac{C_s^R f_s^R + C_L^R \overline{f_L'}}{f_d} \qquad [A10]$$

where C_s^R, C_L^R, and f_s^R are given by Eqs. [A1] and [A2]. Curve (2) in Figure 8 is a plot of the calculated $\overline{C_{sd}}$ *vs* undercooling and represents an upper bound on the expected minimum measured solute composition.

ACKNOWLEDGMENTS

The authors would like to express their gratitude to NASA for support of this work under Grant Nos. NSG 7645 and NAG3-597 through Dr. R. E. Halpern and Mr. F. H. Harf. Discussions during the course of this work with Pro-

fessor T. Z. Kattamis of the University of Connecticut and Professor G. J. Abbaschian of the University of Florida have been helpful.

REFERENCES

1. Y. Wu, T. J. Piccone, Y. Shiohara, and M. C. Flemings: *Metall. Trans. A*, 1987, vol. 18A, pp. 915-24.
2. T. J. Piccone, Y. Wu, Y. Shiohara, and M. C. Flemings: *Metall. Trans. A*, 1987, vol. 18A, pp. 925-32.
3. J. L. Walker: *Physical Chemistry of Process Metallurgy*, G. R. St. Pierre, ed., AIME, 1961, pp. 845-53.
4. T. Z. Kattamis and M. C. Flemings: *Trans. AIME*, 1966, vol. 236, pp. 1523-32.
5. T. Z. Kattamis and M. C. Flemings: *Trans. AFS*, 1967, vol. 75, pp. 191-98.
6. T. Z. Kattamis and M. C. Flemings: *Metall. Trans.*, 1970, vol. 1, pp. 1449-51.
7. S. Skolianos, P. S. Liu, and T. Z. Kattamis: *Grain Refinement in Castings and Welds*, G. J. Abbaschian and S. A. David, eds., AIME, 1983, pp. 97-116.
8. C. G. Levi and R. Mehrabian: *Undercooled Alloy Phases*, E. W. Collings and C. C. Koch, eds., AIME, 1987, pp. 345-74.
9. T. Z. Kattamis and M. C. Flemings: *Mod. Cast.*, 1967, vol. 52, p. 819.
10. T. Z. Kattamis: *Z. Metallkunde*, 1970, vol. 61, pp. 856-60.
11. D. D. McDevitt and G. J. Abbaschian: *Chemistry and Physics of Rapidly Solidified Materials*, B. J. Berkowitz and R. O. Scattergood, eds., AIME, 1983, pp. 49-61.
12. W. J. Boettinger, S. R. Coriell, and R. F. Sekerka: *Mat. Sci. Eng.*, 1984, vol. 65, p. 27.
13. J. C. Baker and J. W. Cahn: *Solidification*, ASM, Metals Park, OH, 1971, pp. 23-58.
14. M. J. Aziz: *J. Appl. Phys.*, 1982, vol. 53, pp. 1158-68.
15. J. H. Perepezko: *Rapid Solidification Processing: Principles and Technologies II*, R. Mehrabian, B. H. Kear, and M. Cohen, eds., Claitor's Publishing Division, 1980, pp. 56-67.
16. M. G. Chu, Y. Shiohara, and M. C. Flemings: *Metall. Trans. A*, 1984, vol. 15A, pp. 1303-10.
17. J. H. Perepezko, Y. Shiohara, J. S. Paik, and M. C. Flemings: *Rapid Solidification Processing: Principles and Technologies III*, R. Mehrabian, ed., NBS, 1982, pp. 28-44.
18. M. G. Chu, R. J. Rioja, G. J. Hildeman, and D. K. Denzer: *Proceedings of the 43rd Annual Meeting of the Electron Microscopy Society of America*, G. W. Bailey, ed., EMSA, 1985, p. 32.
19. M. Yamamoto, Y. Wu, Y. Shiohara, and M. C. Flemings: *Rapidly Solidified Alloys and Their Mechanical and Magnetic Properties*, B. C. Giessen, D. E. Polk, and A. I. Taub, eds., MRS, 1986, pp. 411-14.
20. W. J. Boettinger, L. Bendersky, and J. G. Early: *Metall. Trans. A*, 1986, vol. 17A, pp. 781-90.
21. D. C. Joy: *Quantitative Scanning Electron Microscopy*, D. B. Holt *et al.*, eds., London Academic Press, 1974, p. 131.
22. D. L. Davidson: *International Metals Review*, 1984, vol. 29, p. 75.
23. S. N. Tewari: *Metall. Trans. A*, 1987, vol. 18A, pp. 525-42.
24. J. E. Hilliard and J. W. Cahn: *Trans. AIME*, 1961, vol. 221, p. 344.